Chinese Journal of
POLYMER SCIENCE

RESEARCH ARTICLE

https://doi.org/10.1007/s10118-024-3082-z
Chinese J. Polym. Sci. **2024**, *42*, 636–642

Ordered Bicontinuous Network Structures Regulated by Orientational Interactions in a Rod-Coil Block Copolymer

Xiao-Lin Lyu[a,b*], Shi-Chu Yang[a], An-Qi Xiao[a], Ping-Ping Hou[a], Wei Zhang[a], Hong-Bing Pan[a], Zhi-Hao Shen[a*], Xing-He Fan[a], and Qi-Feng Zhou[a]

[a] *Beijing National Laboratory for Molecular Sciences, Key Laboratory of Polymer Chemistry and Physics of Ministry of Education, College of Chemistry and Molecular Engineering, Peking University, Beijing 100871, China*
[b] *Key Laboratory of Advanced Materials Technologies, International (HongKong Macao and Taiwan) Joint Laboratory on Advanced Materials Technologies, College of Materials Science and Engineering, Fuzhou University, Fuzhou 350108, China*

Electronic Supplementary Information

Abstract The rich phase behavior of block copolymers (BCPs) has drawn great attention in recent years. However, the double diamond (DD) phase is rarely obtained because of the competition between the minimization of interfacial energy and packing frustration. Here, a rod-coil BCP containing mesogen-jacketed liquid crystalline polymer is designed to acquire ordered bicontinuous network nanostructures. The reduction of internal energy originating from the orientational interaction among the rod blocks can compensate for the free energy penalty of packing frustration to stabilize the DD structure. The resulting BCP can also experience lamellae-to-DD and double gyroid-to-lamellae transitions by changing the annealing temperature. These results make the rod-coil BCP an excellent candidate for the self-assembly of ordered network structures, demonstrating great potential in nanopatterning and metamaterials.

Keywords Block copolymer; Rod-coil; Ordered bicontinuous phase; Double diamond; Double gyroid

Citation: Lyu, X. L.; Yang, S. C.; Xiao, A. Q.; Hou, P. P.; Zhang, W.; Pan, H. B.; Shen, Z. H.; Fan, X. H.; Zhou, Q. F. Ordered bicontinuous network structures regulated by orientational interactions in a rod-coil block copolymer. *Chinese J. Polym. Sci.* **2024**, *42*, 636–642.

INTRODUCTION

The self-assembly of block copolymers (BCPs) has drawn great attention in recent decades because of its potential in nanopatterning, metamaterials, *etc*.[1–6] The structures of BCPs rely on three parameters, the volume fraction (f) of a component in the BCP, the Flory-Huggins interaction parameter (χ) between the two components, and the total degree of polymerization (N).[7,8] They can form hexagonally-packed cylinders (HEX), lamellae (LAM), body-centered cubic arrays of spheres (BCC), and double gyroid (DG) through microphase separation.[9–13] However, another ordered bicontinuous structure, double diamond (DD), can rarely be obtained by self-assembly using BCPs.

Generally, the DD phase with 4-fold nodes and $Pn\bar{3}m$ symmetry is regarded as an unstable or metastable morphology compared with BCC, HEX, LAM, and DG because of competition between the minimization of interfacial energy and packing frustration.[14–16] The minimization of interfacial energy tends to form structures with a constant mean curvature (CMC) surface. DD and DG, which are common in lipids and amphiphilic surfactants, are composed of two separated interpenetrating networks in a continuous matrix with a CMC-like surface (the Schwarz diamond surface and the Schoen gyroid surface respectively).[17–19] However, packing frustration tends to form microdomains with uniform thickness, and thus the blocks do not have to fill up space with excessive stretching.[20] Therefore, domain interfaces with non-uniform thicknesses would deviate from the complex CMC surface to generate more domains with a uniform thickness and reduce packing frustration to stabilize bicontinuous nanostructures.

The reduction in packing frustration can compensate for the increased interfacial energy originating from a non-CMC surface. Therefore, the degree of deviation from the CMC surface can measure the stability of these complex structures. The calculated interface of DG deviates less from the CMC surface than that of DD.[21] Finally, DG is more stable when the interfacial energy minimization and packing frustration achieve an equilibrium. Matsen and Escobedo *et al*. further theoretically confirmed the above mechanism using diblock/homopolymer blends.[22–24] Recently, although DD structures have been acquired by solution assembly of amphiphilic BCPs,[25–28] blending strategy,[15,29,30] or introduction of chiral chains[31,32] to minimize packing frustration, it is still a challenge to obtain DD structure in the bulk self-assembly of neat BCPs.

* Corresponding authors, E-mail: lyuxiaolin@fzu.edu.cn (X.L.L.)
E-mail: zshen@pku.edu.cn (Z.H.S.)

Received November 9, 2023; Accepted December 21, 2023; Published online January 28, 2024

Herein, we report ordered bicontinuous phases, DD and DG, formed by a rod-coil BCP composed of the flexible polydimethylsiloxane (PDMS) and the rigid mesogen-jacketed liquid crystalline polymer (MJLCP) poly{2,5-bis[(4-methoxyphenyl)-oxycarbonyl]styrene} (PMPCS). The interplay between the microphase separation of the two blocks and the orientational interaction of the rod blocks makes its phase behavior different from that of regular coil-coil BCPs and stabilizes the DD structure by reducing internal energy to make up for the packing frustration. The LAM-to-DD and DG-to-LAM phase transitions can also be observed by changing the annealing temperature, demonstrating dramatic changes in the phase behavior from the variation in the segregation strength. This work can promote the development of ordered bicontinuous structures in BCPs and show great potential in nanotemplates, nanoporous materials, and metamaterials.

EXPERIMENTAL

Synthesis and Characterization of the Macroinitiator and PDMS-*b*-PMPCS

The synthetic route of the macroinitiator 2-bromoisobutyrate-terminated PDMS was shown in Scheme S1 and Fig. S1 (in the electronic supplementary information, ESI). The absolute molecular weight (MW) of the macroinitiator was determined by matrix-assisted laser desorption/ionization time of flight mass spectrometry (MALDI-TOF-MS) (Fig. S2 in ESI). PDMS-*b*-PMPCS was prepared by atom-transfer radical polymerization (Scheme S1 in ESI). The molar mass dispersity ($Đ_M$) of the macroinitiator and PDMS-*b*-PMPCS was determined by size exclusion chromatography (SEC) (Figs. S3 and S4 in ESI), and the DP of PMPCS was determined by the absolute MW of the macroinitiator and the ^{1}H-NMR result (Fig. S5 in ESI). The volume fraction of PMPCS, f_{rod}, was calculated assuming the densities of PDMS and PMPCS are 0.97 and 1.28 g/cm^3, respectively.

Sample Preparation

Bulk samples of PDMS-*b*-PMPCS block copolymers were prepared through solution casting from tetrahydrofuran (THF) solutions overnight and then annealed at 130 and 190 °C for 2 days. Then, liquid nitrogen was used to quench the samples in order to maintain the high-temperature structures. After the small-angle X-ray scattering (SAXS) and wide-angle X-ray scattering (WAXS) experiments, the samples were embedded in epoxy resins and microtomed with a thickness of approximately 100 nm by an ultramicrotome for transmission electron microscopy (TEM) observation.

Instruments

^{1}H-NMR spectra were conducted on a Bruker-400 (400 MHz) spectrometer. The GPC experiments were performed on a Waters 1515 instrument with an isocratic HPLC pump and a Waters 2414 instrument with a refractive index detector using THF as eluant (1 mL/min). The polystyrenes were used as standards to plot the calibration curve. MALDI-TOF-MS results were obtained on an AB Sciex 5800 instrument. The SAXS and WAXS experiments were carried out on Xeuss 2.0 (Xenocs SA, France) at Institute of Chemistry, Chinese Academy of Sciences (ICCAS), the synchrotron X-ray beamline 1W2A at Beijing Synchrotron Radiation Facility (BSRF), and the synchrotron X-ray beamline BL16B1 at Shanghai Synchrotron Radiation Facility (SSRF).[33,34] The wavelength of the X-ray beam was 0.154 nm. The scattering angles were calibrated with silver behenate. The bright field TEM images were acquired with a Tecnai F20 transmission electron microscopy at an accelerating voltage of 200 kV.

RESULTS AND DISCUSSION

The characterization results of PDMS-*b*-PMPCS are listed in Table 1. The nanostructures were determined by synchrotron small-angle X-ray scattering (SAXS) and transmission electron microscopy (TEM) experiments. The SAXS profile of $D_{65}M_{20}$ with an annealing temperature of 130 °C exhibits a scattering vector ratio of 1:2:3, indicative of a LAM nanostructure (Fig. 1a). The primary scattering peak is at q^*=0.374 nm^{-1} with a *d*-spacing of 16.8 nm. The TEM micrograph of $D_{65}M_{20}$ annealed at 130 °C confirms the LAM nanostructure (Fig. 1b). The layer spacing obtained from the TEM image is approximately 16.9 nm, consistent with the SAXS result within the experimental error. Because the electron density of PDMS is higher than that of PMPCS, the dark part in the image is the PDMS domain, while the bright part belongs to the PMPCS domain. According to the f_{rod} and *d*-spacing values of the LAM structure, the spacing of the PMPCS layer is 16.9 nm × 56% = 9.5 nm, in agreement with that of the bright part in the TEM image (approximately 10.8 nm). The PMPCS rods are supposed to arrange in a double-layer manner because the length of the PMPCS rod with all-*trans* conformation is about 5.0 nm. The schematic diagram of the LAM structure is shown in Fig. 1(c).

As described in the literature, ordered network nanostructures such as DD, DG, and *Fddd* can be regulated through the self-assembly of BCPs. The scattering vector ratio of $D_{65}M_{20}$ with the annealing temperature of 190 °C is $2^{1/2}$:$3^{1/2}$:$4^{1/2}$:$6^{1/2}$:$8^{1/2}$, which is consistent with that of the DD phase (Fig. 2a). To avoid confusion with DG and *Fddd*, the theoretical diffraction peak positions of these two network phases are labeled with blue and red lines in Fig. 2(a) by fixing the primary peak position. It can be found that the high-order diffraction peaks of the DG phase do not match with those in the SAXS result. Meanwhile, although the second, fourth, and fifth peaks in the SAXS result appear in the theoretical peaks of the *Fddd* phase, the third peak in the SAXS result does not

Table 1 Characterization and phase structures of PDMS-*b*-PMPCS.

Sample	$M_{n,D}$ [a] (kg/mol)	$M_{n,M}$ [b] (kg/mol)	$Đ_M$ [a] (M_w/M_n)	$f_{rod's}$	Nanostructure [c] (130 °C)	Nanostructure [c] (190 °C)
$D_{65}M_{20}$	4.9	8.1	1.11	0.56	LAM	DD
$D_{65}M_{34}$	4.9	13.7	1.17	0.68	DG	DG + LAM

[a] Determined by SEC in THF, $M_{n,D}$ is the number-averaged MW of the PDMS block and $Đ_M$ is the molar mass dispersity of the BCP; [b] Determined by ^{1}H-NMR, $M_{n,M}$ is the number-averaged MW of the PMPCS block; [c] The nanostructures were characterized by SAXS and TEM.

https://doi.org/10.1007/s10118-024-3082-z

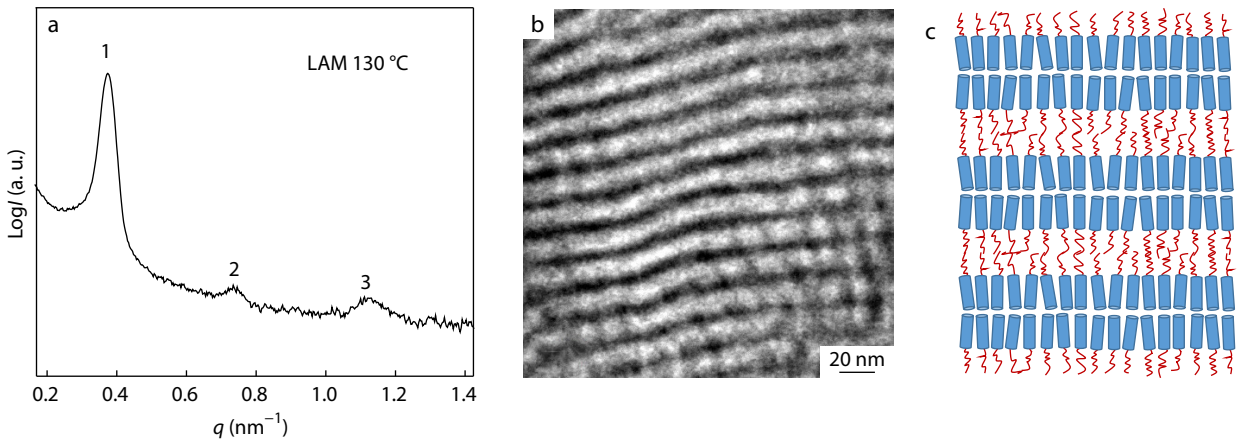

Fig. 1 (a) SAXS profile, (b) TEM micrograph, and (c) schematic illustration of the LAM phase self-assembled by $D_{65}M_{20}$ at 130 °C. The blue and red colors represent PMPCS and PDMS blocks, respectively.

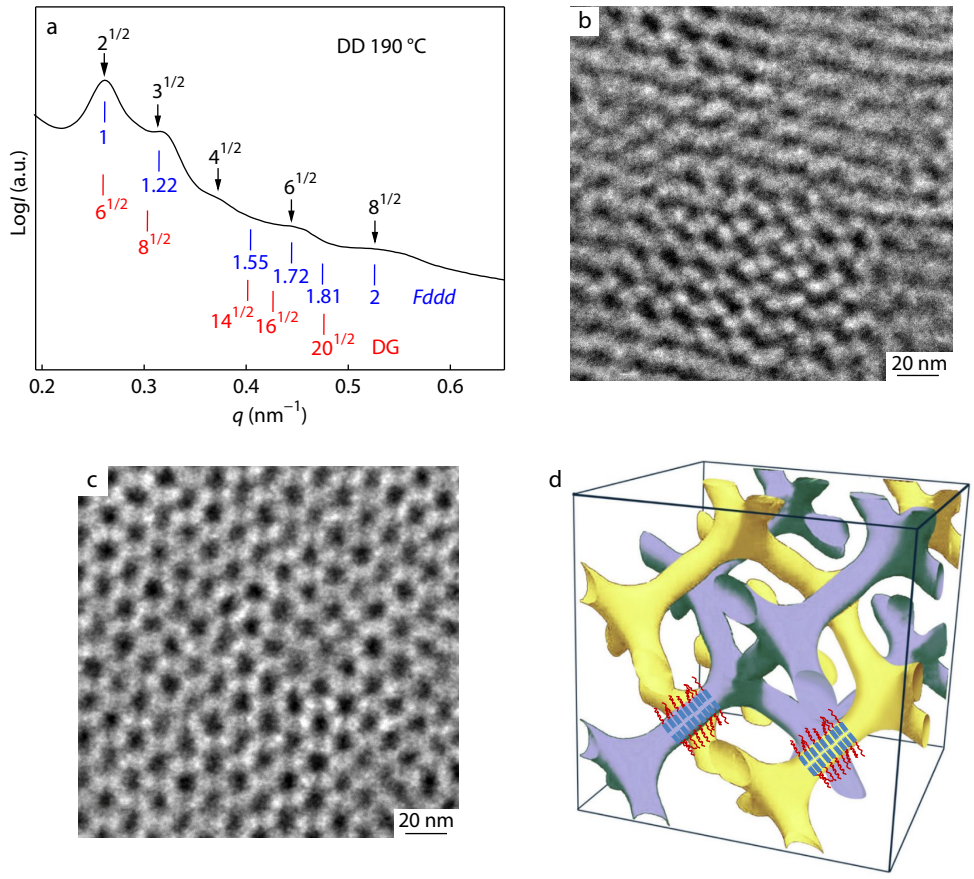

Fig. 2 SAXS profile of the DD phase self-assembled by $D_{65}M_{20}$ at 190 °C with the blue and red lines representing the theoretical diffraction peak positions of *Fddd* and DG phases, respectively (a); TEM micrographs (b, c) and schematic illustration (d) of the DD phase. The blue and red colors represent PMPCS and PDMS blocks, respectively.

belong to the *Fddd* phase. In addition, the theoretical third and fifth peaks of the *Fddd* phase do not appear in the SAXS profile. Therefore, the structure of $D_{65}M_{20}$ self-assembling at 190 °C can be identified as the DD phase, with the peaks corresponding to the (110), (111), (200), (211), and (220) diffractions. The sample was also annealed at 190 °C for 96 h to verify the stability of the DD nanostructure, and the result remained the same. To further confirm the DD nanostructure, we conducted TEM experiments. The TEM micrographs display a helical pattern from the [1$\bar{1}$1] projection (Fig. 2b) and a hexagonal pattern from the [111] projection (Fig. 2c) of a DD lattice.[35,36] The distance between the adjacent dark domains is approximately 18.8 nm (Fig. 2c). The *d*-spacing of the $(111)_{DD}$ plane is determined to be 20.3 nm (q=0.309 nm^{-1}) according to the second peak in the SAXS profile, in agreement with the TEM result within the margin of errors.

https://doi.org/10.1007/s10118-024-3082-z

Based on the above results, the LAM structure should be the most stable structure at low temperatures. At high temperatures, the LAM structure is likely to be unstable because the thermal motion of the coil block increases and large interfacial areas between the layers are required to relieve the free energy of deformation originating from the coil packing.[37] As a result, the LAM structure would break down into a new nanostructure DD with $Pn\bar{3}m$ symmetry. To understand the reason for the phase transition, WAXS experiments were carried out (Fig. S6 in ESI). In rod-coil BCPs, the other two parameters, the geometrical asymmetry interaction (ν) and the orientational interaction (μ), can also influence the structures. The liquid crystalline (LC) phase behavior of PMPCS is MW-dependent, and PMPCS rods in $D_{65}M_{20}$ are in the amorphous state during the annealing temperature range, which means that the strength of the orientational interaction among PMPCS rods remains unchanged. However, the decrease of the Flory-Huggins interaction parameter and the corresponding χN value will weaken the segregation strength between the two blocks when the annealing temperature is increased, and then the structure of $D_{65}M_{20}$ will have an order-order transition (OOT). Similar to the situation in *s*PP-*b*-PS that the ordered packing of helical *s*PP segments can reduce internal energy to make up for the packing frustration in the 4-fold node caused by the entropic loss of the stretched polymer chains,[36] the orientational interaction of PMPCS can also decrease the internal energy to stabilize the DD structure. Based on the above analysis, the schematic illustration of the DD phase is shown in Fig. 2(d), with the PMPCS rods forming two interpenetrating networks and the PDMS coils forming the continuous matrix. Therefore, unlike the DG and *Fddd* phases that were previously reported in PDMS-*b*-PMPCS,[38] we further identify the DD structure as well as the infrequent OOT between the DD and lamellar phases by modulating the MW of PDMS and the orientation interactions of PMPCS, which have rarely been observed in other literature.

To further investigate the role of the orientational interaction among PMPCS rods on the phase behavior, the MW of PMPCS is increased to allow the formation of an LC phase upon annealing. The peaks of $D_{65}M_{34}$ annealed at 130 °C exhibit a scattering vector ratio of $6^{1/2}$:$8^{1/2}$:$16^{1/2}$:$24^{1/2}$:$32^{1/2}$:$42^{1/2}$, which coincides with that of the DG phase (Fig. 3a).

The peaks can be assigned as the (211), (220), (400), (422), (440), and (541) diffractions. The DG structure can be further confirmed by TEM results (Figs. 3b and 3c). According to the volume fraction of PMPCS, it can be speculated that the PDMS coils form two interpenetrating networks and the PMPCS rods form the continuous matrix. The cross-sectional view of the molecular arrangement of the 3-fold node in the DG structure is shown in Fig. 3(d).

With the annealing temperature rising to 190 °C, the intensities of the abovementioned peaks decrease, and several

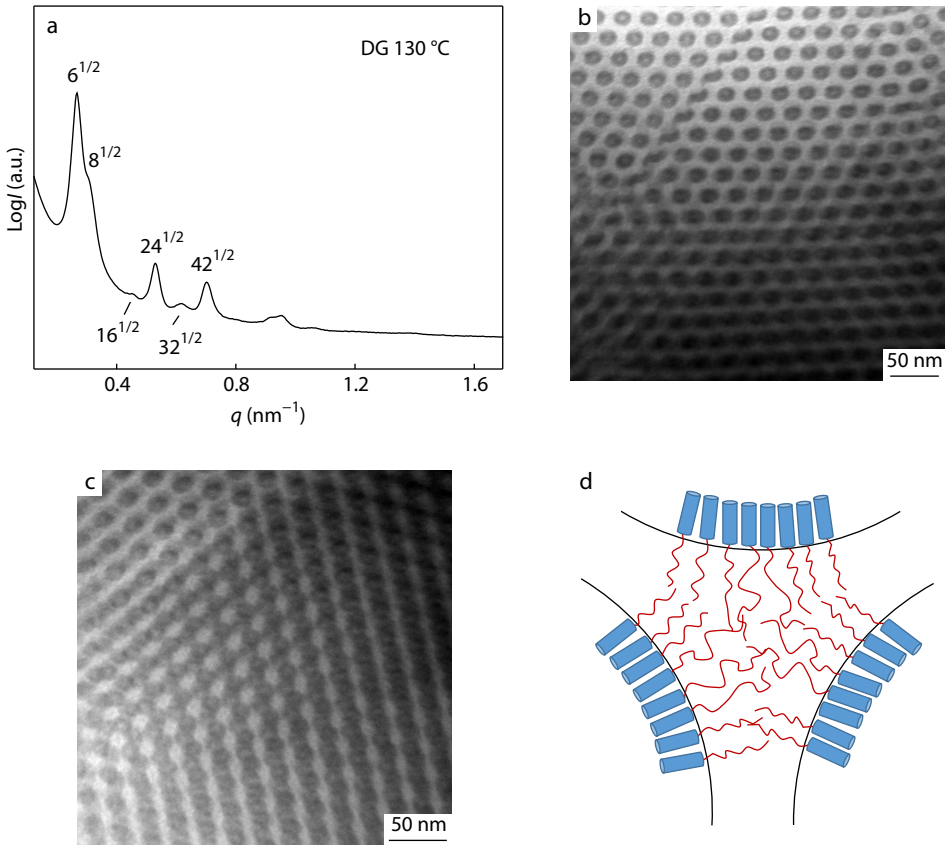

Fig. 3 SAXS profile (a) and TEM micrographs (b, c) of the DG phase self-assembled by $D_{65}M_{34}$ at 130 °C and cross-sectional view of possible molecular arrangement of the 3-fold node in the DG structure (d). The blue and red colors represent PMPCS and PDMS blocks, respectively.

https://doi.org/10.1007/s10118-024-3082-z

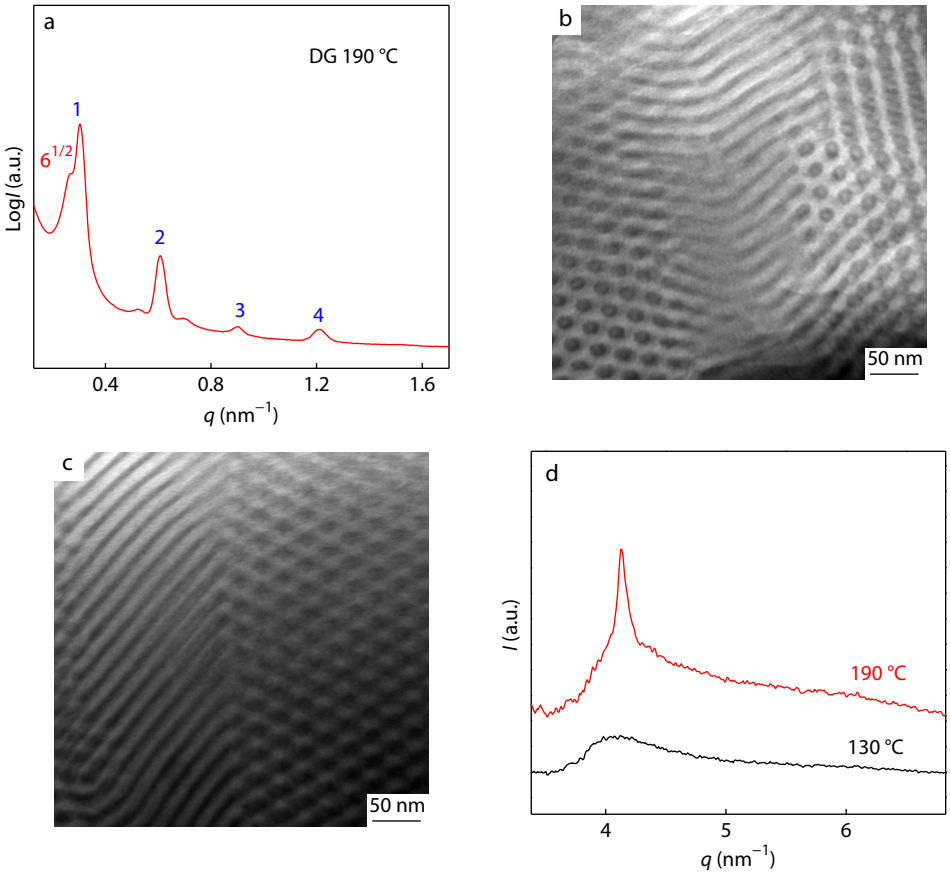

Fig. 4 SAXS profile (a) and TEM micrographs (b, c) of $D_{65}M_{34}$ after thermal annealing at 190 °C and WAXS profiles of $D_{65}M_{34}$ after thermal annealing at 130 and 190 °C (d).

new peaks with the scattering vector ratio of 1:2:3:4 appear (Fig. 4a). That is, the DG structure and the LAM structure coexist at the annealing temperature of 190 °C, which can also be verified by TEM (Figs. 4b and 4c). The above results reveal that the structure of $D_{65}M_{34}$ can gradually transform from DG to LAM with increasing temperature. Considering the MW-dependent LC phase behavior of PMPCS, WAXS experiments were conducted to study whether the liquid crystallinity of PMPCS triggered the OOT. As shown in Fig. 4(d), the LC phase of the rod block forms at the annealing temperature of 190 °C with a sharp peak (q=4.14 nm^{-1}). The formation of the LC phase will induce the PMPCS blocks to be more rigid, and then the strength of the orientational interaction among PMPCS rods will be increased. Therefore, although the Flory-Huggins interaction parameter between the two blocks is decreased when the annealing temperature is increased, the enhancement in the orientational interaction of PMPCS caused by the formation of the LC phase will increase the whole effective segregation strength.[39,40] Meanwhile, the more rigid PMPCS will also increase the geometrical asymmetry between the two blocks. At last, DG will be unstable after thermal annealing at 190 °C because of relatively large interfacial curvature, and gradually transforms into LAM with low interfacial curvature. Thus, the OOT of $D_{65}M_{34}$ with increasing temperature is mainly caused by the LC formation of PMPCS rods in the outward matrix.

As mentioned above, the microstructures of rod-coil BCPs are influenced by not only f and χN but also the geometrical asymmetry interaction and orientational interaction. The phase diagram is shown in Fig. S7 (in ESI). When the MW of PMPCS is lower than the critical MW for LC formation, the segregation strength between the two blocks will be decreased because of the decrease in the Flory-Huggins interaction parameter with increasing annealing temperature. When the MW of PMPCS exceeds the critical MW, the segregation strength between the two blocks will be enhanced mainly owing to the increase in the orientational interaction of PMPCS and geometrical asymmetry between the two blocks caused by LC formation. The enhanced segregation strength caused by the formation of LC phase can also be observed in the BCP containing side-chain liquid crystalline polymers, which promotes the formation of low-curvature structures (*e.g.*, BCC, HEX, and LAM), instead of DD.[41] According to the theoretical results,[42–45] the network structures generally exist in the weak-segregation region while the structures with low interfacial curvatures (*e.g.*, BCC, HEX, and LAM) exist in the strong-segregation region. Therefore, the OOTs of $D_{65}M_{20}$ and $D_{65}M_{34}$ are also in accord with the theoretical results.

CONCLUSIONS

In conclusion, the rich structures of PDMS-*b*-PMPCS are studied because the geometrical asymmetry and orientational interaction play an important role in the self-assembly of rod-coil BCPs.

https://doi.org/10.1007/s10118-024-3082-z

By changing the MW of the rod block and annealing temperature, the BCP can self-assemble into LAM, DD, and DG nanostructures. In addition, for the first time the DD structure and a LAM-to-DD transition are observed in the bulk sample of a BCP containing the rigid MJLCP. The orientational interaction of PMPCS can reduce internal energy to minimize packing frustration for stabilizing the DD structure. Moreover, the transformation of PMPCS from the amorphous to the LC phase also induces a phase transition from DG to LAM. Therefore, various nanostructures, especially bicontinuous network structures (such as DD and DG), can be easily obtained in the rod-coil BCPs containing MJLCP rod blocks. Meanwhile, it is also a promising candidate to be used as nanotemplates, nanoporous materials, and metamaterials.

Conflict of Interests

The authors declare no interest conflict.

Electronic Supplementary Information

Electronic supplementary information (ESI) is available free of charge in the online version of this article at http://doi.org/10.1007/s10118-024-3082-z.

Data Availability Statement

The data that support the findings of this study are available from the corresponding author upon reasonable request. The author's contact information: lyuxiaolin@fzu.edu.cn (X.L.L.), zshen@pku.edu.cn (Z.H.S.).

ACKNOWLEDGMENTS

This work was financially supported by the National Natural Science Foundation of China (Nos. 51921002, 22203015 and 51725301), Natural Science Foundation of Fujian Province (No. 2021J01591), and the National Key R&D Program of China (No. 2018YFB0703702). The suggestions and help offered by Prof. Rong-Ming Ho of National Tsing Hua University are greatly appreciated. The authors acknowledge the scientists at the synchrotron X-ray beamline 1W2A at Beijing Synchrotron Radiation Facility (BSRF) and the synchrotron X-ray beamline BL16B1 at Shanghai Synchrotron Radiation Facility (SSRF) for their assistance on the SAXS experiments.

REFERENCES

1 Jeon, H. I.; Jo, S.; Jeon, S.; Jun, T.; Moon, J.; Cho, J. H.; Ahn, H.; Lee, S.; Ryu, D. Y.; Russell, T. P. Repairable macroscopic monodomain arrays from block copolymers enabled by photoplastic and photodielectric effects. *ACS Nano* **2023**, *17*, 8367–8375.
2 Kuo, S. W. Construction archimedean tiling patterns based on soft materials from block copolymers and covalent organic frameworks. *Giant* **2023**, *15*, 100170.
3 Sadek, H.; S, K. S.; Wang, C. W.; Lee, C. C.; Chang, S. Y.; Ho, R. M. Bioinspired nanonetwork hydroxyapatite from block copolymer templated synthesis for mechanical metamaterials. *ACS Nano* **2022**, *16*, 18298–18306.
4 Sadek, H.; Siddique, S. K.; Wang, C. W.; Chiu, P. T.; Lee, C. C.; Ho, R. M. Starfish-inspired diamond-structured calcite single crystals from a bottom-up approach as mechanical metamaterials. *ACS Nano* **2023**, *17*, 15678–15686.
5 Xu, G.; Li, M.; Wang, Q.; Feng, F.; Lou, Q.; Hou, Y.; Hui, J.; Zhang, P.; Wang, L.; Yao, L.; Qin, S.; Ouyang, X.; Wu, D.; Ling, D.; Wang, X. A dual-kinetic control strategy for designing nano-metamaterials: novel class of metamaterials with both characteristic and whole sizes of nanoscale. *Adv. Sci.* **2023**, *10*, e2205595.
6 Yang, W.; Liu, D.; Liu, Y.; Yang, S.; Liu, Y.; Shen, Z.; Yang, H.; Fan, X. H.; Zhou, Q. F. Large-area uniaxially oriented sub-5 nm line patterns of hybrid liquid crystals constructed by perylene diimide and oligo(dimethylsiloxane). *Chem. Eur. J.* **2023**, *29*, e202203702.
7 Kim, I.; Li, S. Recent progress on polydispersity effects on block copolymer phase behavior. *Polym. Rev.* **2019**, *59*, 561–587.
8 Wong, C. K.; Qiang, X.; Müller, A. H. E.; Gröschel, A. H. Self-assembly of block copolymers into internally ordered microparticles. *Prog. Polym. Sci.* **2020**, *102*, 101211.
9 Cui, S.; Zhang, B.; Shen, L.; Bates, F. S.; Lodge, T. P. Core-shell gyroid in ABC bottlebrush block terpolymers. *J. Am. Chem. Soc.* **2022**, *144*, 21719–21727.
10 Hou, L.; Xu, Z.; Li, W. Largely tunable morphologies self-assembled by $A(AB)_n$ miktoarm star copolymer in solutions. *Macromolecules* **2023**, *56*, 3440–3453.
11 Kang, S.; Lee, J.; Yoon, H.; Jang, J.; Kim, E.; Kim, J. K. Tetragonally packed inverted cylindrical microdomains from binary block copolymer blends with enhanced hydrogen bonding. *ACS Macro Lett.* **2023**, *12*, 915–920.
12 Ma, Z.; Zhou, D.; Xu, M.; Gan, Z.; Zheng, T.; Wang, S.; Tan, R.; Dong, X. H. Discrete linear-branched block copolymer with broken architectural symmetry. *Macromolecules* **2023**, *56*, 833–840.
13 Mishra, A. K.; Lee, J.; Kang, S.; Kim, E.; Choi, C.; Kim, J. K. Gallol-based block copolymer with a high Flory-Huggins interaction parameter for next-generation lithography. *Macromolecules* **2022**, *55*, 10797–10803.
14 Thomas, E. L.; Anderson, D. M.; Henkee, C. S.; Hoffman, D. Periodic area-minimizing surfaces in block copolymers. *Nature* **1988**, *334*, 598–601.
15 Chu, C. Y.; Pei, R. Y.; Chen, H. L. Order-order transition from ordered bicontinuous double diamond to hexagonally packed cylinders in stereoregular diblock copolymer/homopolymer blends. *Macromolecules* **2018**, *51*, 8493–8500.
16 Liu, C. Y.; Chen, H. L. Undulating the lamellar interface of polymer-surfactant complex by dendrimer. *Macromolecules* **2017**, *50*, 6501–6508.
17 Feng, X.; Dimitriyev, M. S.; Thomas, E. L. Soft, malleable double diamond twin. *Proc. Natl. Acad. Sci. U. S. A.* **2023**, *120*, e2213441120.
18 Yang, K. C.; Reddy, A.; Tsai, H. W.; Zhao, W.; Grason, G. M.; Ho, R. M. Breaking mirror symmetry of double gyroids *via* self-assembly of chiral block copolymers. *ACS Macro Lett.* **2022**, *11*, 930–934.
19 Feng, X.; Burke, C. J.; Zhuo, M.; Guo, H.; Yang, K.; Reddy, A.; Prasad, I.; Ho, R. M.; Avgeropoulos, A.; Grason, G. M.; Thomas, E. L. Seeing mesoatomic distortions in soft-matter crystals of a double-gyroid block copolymer. *Nature* **2019**, *575*, 175–179.
20 Reddy, A.; Feng, X.; Thomas, E. L.; Grason, G. M. Block copolymers beneath the surface: measuring and modeling complex morphology at the subdomain scale. *Macromolecules* **2021**, *54*, 9223–9257.
21 Matsen, M. W.; Bates, F. S. Origins of complex self-assembly in block copolymers. *Macromolecules* **1996**, *29*, 7641–7644.
22 Martinez-Veracoechea, F. J.; Escobedo, F. A. Bicontinuous phases in diblock copolymer/homopolymer blends: simulation and self-consistent field theory. *Macromolecules* **2009**, *42*, 1775–1784.

23 Martinez-Veracoechea, F. J.; Escobedo, F. A. Monte Carlo study of the stabilization of complex bicontinuous phases in diblock copolymer systems. *Macromolecules* **2007**, *40*, 7354–7365.
24 Matsen, M. W. Phase-behavior of block-copolymer homopolymer blends. *Macromolecules* **1995**, *28*, 5765–5773.
25 Chen, H.; Fan, Y.; Zhang, N.; Trepout, S.; Ptissam, B.; Brulet, A.; Tang, B. Z.; Li, M. H. Fluorescent polymer cubosomes and hexosomes with aggregation-induced emission. *Chem. Sci.* **2021**, *12*, 5495–5504.
26 Lyu, X.; Tang, Z.; Xiao, A.; Zhang, W.; Pan, H.; Shen, Z.; Fan, X. H. Temperature-controlled formation of inverse mesophases assembled from a rod-coil block copolymer. *Polym. Chem.* **2019**, *10*, 6031–6036.
27 Lv, F.; An, Z.; Wu, P. Scalable preparation of alternating block copolymer particles with inverse bicontinuous mesophases. *Nat. Commun.* **2019**, *10*, 1397.
28 Lyu, X.; Xiao, A.; Zhang, W.; Hou, P.; Gu, K.; Tang, Z.; Pan, H.; Wu, F.; Shen, Z.; Fan, X. H. Head-tail asymmetry as the determining factor in the formation of polymer cubosomes or hexasomes in a rod-coil amphiphilic block copolymer. *Angew. Chem. Int. Ed.* **2018**, *57*, 10132–10136.
29 Li, Q.; Woo, D.; Kim, J. K.; Li, W. Truly "inverted" cylinders and spheres formed in the $A(AB)_3$/AC blends of B/C hydrogen bonding interactions. *Macromolecules* **2022**, *55*, 6525–6535.
30 Takagi, H.; Yamamoto, K. Effect of block copolymer composition and homopolymer molecular weight on ordered bicontinuous double-diamond structures in binary blends of polystyrene-polyisoprene block copolymer and polyisoprene homopolymer. *Macromolecules* **2021**, *54*, 5136–5143.
31 Lin, C. H.; Higuchi, T.; Chen, H. L.; Tsai, J. C.; Jinnai, H.; Hashimoto, T. Stabilizing the ordered bicontinuous double diamond structure of diblock copolymer by configurational regularity. *Macromolecules* **2018**, *51*, 4049–4058.
32 Chiu, P. T.; Sung, Y. C.; Yang, K. C.; Tsai, J. C.; Wang, H. F.; Ho, R. M. Curving and twisting in self-assembly of triblock terpolymers driven by a chiral end block. *Macromolecules* **2022**, *55*, 1185–1195.
33 Li, Z.; Wu, Z.; Mo, G.; Xing, X.; Liu, P. A small-angle X-ray scattering station at beijing synchrotron radiation facility. *Instrum. Sci. Technol.* **2014**, *42*, 128–141.
34 Tian, F.; Li, X. H.; Wang, Y. Z.; Yang, C. M.; Zhou, P.; Lin, J. Y.; Zeng, J. R.; Hong, C. X.; Hua, W. Q.; Li, X. Y.; Miao, X. R.; Bian, F. G.; Wang, J. Small angle X-ray scattering beamline at SSRF. *Nucl. Sci. Tech.* **2015**, *26*, 030101.
35 Chu, C. Y.; Jiang, X.; Jinnai, H.; Pei, R. Y.; Lin, W. F.; Tsai, J. C.; Chen, H. L. Real-space evidence of the equilibrium ordered bicontinuous double diamond structure of a diblock copolymer. *Soft Matter* **2015**, *11*, 1871–1876.
36 Chu, C. Y.; Lin, W. F.; Tsai, J. C.; Lai, C. S.; Lo, S. C.; Chen, H. L.; Hashimoto, T. Order-order transition between equilibrium ordered bicontinuous nanostructures of double diamond and double gyroid in stereoregular block copolymer. *Macromolecules* **2012**, *45*, 2471–2477.
37 Lee, M.; Cho, B. K.; Kim, H.; Yoon, J. Y.; Zin, W. C. Self-organization of rod-coil molecules with layered crystalline states into thermotropic liquid crystalline assemblies. *J. Am. Chem. Soc.* **1998**, *120*, 9168–9179.
38 Shi, L. Y.; Zhou, Y.; Fan, X. H.; Shen, Z. Remarkably rich variety of nanostructures and order-order transitions in a rod-coil diblock copolymer. *Macromolecules* **2013**, *46*, 5308–5316.
39 Gao, J.; Tang, P.; Yang, Y. Non-lamellae structures of coil-semiflexible diblock copolymers. *Soft Matter* **2013**, *9*, 69–81.
40 Olsen, B. D.; Shah, M.; Ganesan, V.; Segalman, R. A. Universalization of the phase diagram for a model rod-coil diblock copolymer. *Macromolecules* **2008**, *41*, 6809–6817.
41 Yu, H.; Kobayashi, T.; Yang, H. Liquid-crystalline ordering helps block copolymer self-assembly. *Adv. Mater.* **2011**, *23*, 3337–3344.
42 Khandpur, A. K.; Forster, S.; Bates, F. S.; Hamley, I. W.; Ryan, A. J.; Bras, W.; Almdal, K.; Mortensen, K. Polyisoprene-polystyrene diblock copolymer phase diagram near the order-disorder transition. *Macromolecules* **1995**, *28*, 8796–8806.
43 Martin, J. M.; Li, W.; Delaney, K. T.; Fredrickson, G. H. SCFT study of diblock copolymer melts in electric fields: selective stabilization of orthorhombic *Fddd* network phase. *Macromolecules* **2018**, *51*, 3369–3378.
44 Wang, Y. C.; Matsuda, K.; Kim, M. I.; Miyoshi, A.; Akasaka, S.; Nishitsuji, S.; Saijo, K.; Hasegawa, H.; Ito, K.; Hikima, T.; Takenaka, M. *Fddd* phase boundary of polystyrene-block-polyisoprene diblock copolymer melts in the polystyrene-rich region. *Macromolecules* **2015**, *48*, 2211–2216.
45 Matsen, M. W.; Bates, F. S. Unifying weak- and strong-segregation block copolymer theories. *Macromolecules* **1996**, *29*, 1091–1098.

https://doi.org/10.1007/s10118-024-3082-z